Available online at www.sciencedirect.com
SCIENCE DIRECT
Journal of Power Sources 157 (2006) 464–470
JOURNAL OF POWER SOURCES
www.elsevier.com/locate/jpowsour

Improvement of electrochemical properties of $LiNi_{0.5}Mn_{1.5}O_4$ spinel material by fluorine substitution

Sung-Woo Oh, Sang-Ho Park, Jung-Hyun Kim, Young Chan Bae, Yang-Kook Sun *

Department of Chemical Engineering, Center for Information and Communication Materials, Hanyang University, Seoul 133-791, Republic of Korea

Received 25 April 2005; accepted 21 July 2005
Available online 13 September 2005

Abstract

$LiNi_{0.5}Mn_{1.5}O_{4-x}F_x$ ($0 \leq x \leq 0.1$) cathodes, synthesized by ultrasonic spray pyrolysis at 900 °C, exhibit superior structural and electrochemical properties. The samples are characterized by X-ray diffraction, scanning electron microscopy, differential scanning calorimetry, and electrochemical measurements. During Li^+ extraction, $LiNi_{0.5}Mn_{1.5}O_{4-x}F_x$ has a smaller lattice variation and area-specific impedance than $LiNi_{0.5}Mn_{1.5}O_4$. This enhances the rate capability, especially at high C-rates. $LiNi_{0.5}Mn_{1.5}O_{4-x}F_x$ also exhibits better resistance than $LiNi_{0.5}Mn_{1.5}O_4$ to attack by HF.

Keywords: Lithium secondary battery; Cathode material; Spray pyrolysis; 5 V spinel; Fluorine substitution; Rate capability

1. Introduction

Presently commercialized lithium-ion batteries use layer-structured $LiCoO_2$ positive electrodes (cathodes). Although $LiCoO_2$ cathodes exhibit excellent performance characteristics, an intensive search for improved cathode materials has been conducted for many years because of the high cost and toxicity of $LiCoO_2$. One of the most attractive cathode materials is the spinel $LiMn_2O_4$ [1–4]. This has received much attention because of its low cost, low toxicity, and relatively high specific energy. Despite such advantages, significant capacity fading during cycling, especially at high temperature, has hindered the commercial use of $LiMn_2O_4$ as a positive active material for lithium secondary batteries. Although the origin of the poor cycling performance is not been fully understood, several possible mechanisms have been suggested [2,5], and include: Jahn-Teller distortion; Mn dissolution at high temperature that originates from the $Mn^{3+/4+}$ redox [6]; changes in the crystal lattice arrangement with cycling [7].

The poor cycling behaviour of $LiMn_2O_4$ can be improved by replacing manganese ions with lithium ions $Li_{1+x}Mn_{2-x}O_4$ [8], or by other metal cations, e.g., $LiM_xMn_{2-x}O_4$ (M = Mg, Ti, Cr, Fe, Co, Ni, Cu, Zn) [9–15]. Furthermore, in the course of these studies, it has been found that some of the substituted spinel manganese oxides have exhibited desired discharge and charge behaviour in the higher 5 V region [10–15]. Anion doping also results in good cycling performances. Sun et al. [16,17] reported that S doping at the oxygen site of $LiAl_{0.24}Mn_{1.76}O_{3.97}S_{0.03}$ has a beneficial effect in that it maintains high capacity in the 4 V region, probably due to the formation of a flexible structure by the S doping, compared with the performance of conventional spinel $LiMn_2O_4$ [18]. Amatucci et al. [19] found that the formation of oxyfluoride, $LiAl_{0.2}Mn_{1.8}O_{3.8}F_{0.2}$, results in enhanced of capacity and its retention during 300 cycles. They explained that these characteristics may be a consequence of the good resistance of fluorides to attack by HF found in the electrolyte. Therefore, this study attempts to synthesize F^- ion doped $LiNi_{0.5}Mn_{1.5}O_{4-x}F_x$ ($0 \leq x \leq 0.1$) materials. The structural and electrochemical properties of the prepared materials are characterized. New fluorine-doped, 5-V spinel $LiNi_{0.5}Mn_{1.5}O_{4-x}F_x$ cathode materi-

* Corresponding author. Tel.: +82 2 2220 0524; fax: +82 2 2282 7329.
E-mail address: swoh75@ihanyang.ac.kr (Y.-K. Sun).

0378-7753/$ – see front matter © 2005 Elsevier B.V. All rights reserved.
doi:10.1016/j.jpowsour.2005.07.056

als, prepared by an ultrasonic spray pyrolysis method, are reported.

2. Experimental

The $LiNi_{0.5}Mn_{1.5}O_{4-x}F_x$ ($x = 0$–1.0) powders were prepared by an ultrasonic spray pyrolysis method. Stoichiometric amounts of nickel nitrate hexahydrate ($Ni(NO_3)\cdot 6H_2O$, Aldrich) and manganese nitrate tetrahydrate ($Mn(NO_3)_2\cdot 4H_2O$, Sigma) salts were dissolved in distilled water. The dissolved solution was added to a continuously agitated, aqueous citric acid solution. The molar concentration of citric acid was fixed at 0.2 M and then NH_4OH was added to the starting solution in order to control the solution at a pH of 7. The starting solution was atomized using an ultrasonic nebulizer with a resonant frequency of 1.7 MHz. The aerosol stream was introduced into a vertical quartz reactor that was heated to 500 °C. The inner diameter and length of the quartz reactor were 50 and 1200 mm, respectively. The flow rate of air used as a carrier gas was 10 L min^{-1}.

The precursor powders were mixed with appropriate amounts of $LiOH\cdot H_2O$ and LiF. The mixture was then softly ground and heated to 900 °C at a heating rate of 1 °C min^{-1}. Powder X-ray diffraction (XRD, Rint-2000, Rigaku, Japan) using Cu Kα radiation was employed to identify the crystalline phase of the synthesized material. The FULLPROF Rietveld program was used for analysis of the powder diffraction patterns [20]. The Particle morphology of the powders after calcination was observed with a scanning electron microscope (SEM, JSM 6400, JEOL, Japan). Atomic absorption spectroscopy analysis (AAS, Vario 6, Analytikjena, Germany) was employed to determine the metal dissolution in diluted HF solution (J.T. Baker). The specific surface areas of the powders were measured by nitrogen adsorption according to the Brunauer–Emmett–Teller method (BET, AS1-A4, Quantachrome, USA).

Galvanostatic charge–discharge cycling was performed on 2032-type coin cells. The cathodes were prepared by blending $LiNi_{0.5}Mn_{1.55}O_{4-x}F_x$, Super P carbon black, and polyvinylidene fluoride (80:10:10) in *N*-methyl-2-pyrrolidone. The slurry was then cast on aluminum foil and dried overnight in a vacuum at 110 °C. Discs were then punched out of the foil. Lithium foil (Cyprus Foote Mineral Co.) was used as an anode. The electrolyte solution was 1 M $LiPF_6$ in a mixture of ethylene carbonate (EC) and diethyl carbonate (DEC) in a 1:1 volume ratio (Cheil Industries Inc., Korea). Charge–discharge measurements were carried out between 3.5 and 5 V (versus Li/Li^+) with a current density of 27 mA g^{-1} at 30 °C. For differential scanning calorimetry (DSC) experiments, the coin cells were charged to 5 V at 27 mA g^{-1}. When the cell reached the desired voltage, the current was stopped for 1 h. Then, the current was applied again, until the desired voltage was reached again. This cycling was repeated five times so that the cell stabilized near the desired voltage. Then, the samples were analyzed by DSC at using a temperature scan rate of 1 °C min^{-1}. The DSC experiments were made in welded, scaled, stainless-steel tubes to prevent leakage of the pressurized electrolyte.

3. Results and discussion

In a previous study [21], we reported that the morphology, crystallinity and electrochemical properties of $LiNi_{0.5}Mn_{1.5}O_4$ cathode material are greatly affected by the synthesis conditions such as the pH value of metal–nitrate starting solution and the calcination temperature. Dense and spherical powders were obtained at pH 7, while hollow particles were obtained at low pH values. Also, when calcined at over 900 °C, $LiNi_{0.5}Mn_{1.5}O_4$ exhibited stable cycleability. From these results, $LiNi_{0.5}Mn_{1.5}O_{4-x}F_x$ ($x = 0$–1.0) powders were synthesized under carefully controlled conditions; namely, adjustment of the pH of the metal–nitrate starting solution with NH_4OH solution (pH 7) and calcination temperature (900 °C).

Scanning electron micrographs of $LiNi_{0.5}Mn_{1.5}O_4$ powders preheated at 500 °C are shown in Fig. 1(a). The powders have dense and spherical morphology with an average particle size of approximately 2 μm. Inspection of the cross-section of partially fragmented particles confirmed that the insides of the particles were densely filled. Micrographs of the $LiNi_{0.5}Mn_{1.5}O_{4-x}F_x$ ($x = 0$–0.1) powders calcined at 900 °C are given in Fig. 1. The fluorine-free $LiNi_{0.5}Mn_{1.5}O_4$ spinel powder has a large particle size distribution (Fig. 1(b)). As the fluorine content increases, $LiNi_{0.5}Mn_{1.5}O_{4-x}F_x$ ($x = 0.05$ and 0.1) powders consist of distinct polygonal particles with a slightly larger particle size than that of the fluorine-free sample, see Fig. 1(c) and (d). This morphological change with fluorine substitution has been reported for $Li[Ni_{1/3}Co_{1/3}Mn_{(1/3-x)}Mg_x]O_{2-y}F_y$ [22]. In that case, a small amount of fluorine substitution led to the development of larger square-shaped particles, which agrees well with the present result. The surface areas of the $LiNi_{0.5}Mn_{1.5}O_{4-x}F_x$ ($x = 0 - 0.1$) powders decrease from 3.79 to 0.98 $m^2\ g^{-1}$ due to the increase in the size of each particle.

The X-ray diffraction patterns of $Li[Ni_{0.5}Mn_{1.5}]O_{4-x}F_x$ powders with the fluorine contents of $x = 0$, 0.05, and 0.1, respectively, are shown in Fig. 2. The XRD patterns of all samples can be indexed by a cubic spinel structure with a space group of $Fd\bar{3}m$. Therefore, it is assumed that Li^+ ions occupy the tetrahedral sites (8*a*), Ni^{2+}, Mn^{4+} ions are randomely located at the octahedral sites (16*d*), and O^{2-} and F^- ions are located at the 32*e* sites. All XRD peaks are quite narrow and indicate that highly crystallized $Li[Ni_{0.5}Mn_{1.5}]O_{4-x}F_x$ species are formed. Only little amounts of NiO secondary phases are detected from the small peaks at $2\theta = 37.8°$, 43.2° and 62.8°.

From the above assumptions, the XRD patterns of the $Li[Ni_{0.5}Mn_{1.5}]O_{4-x}F_x$ species were refined by a space group of $Fd\bar{3}m$. Upon refinement, however, the fluorine was not considered because significant errors were encountered dur-

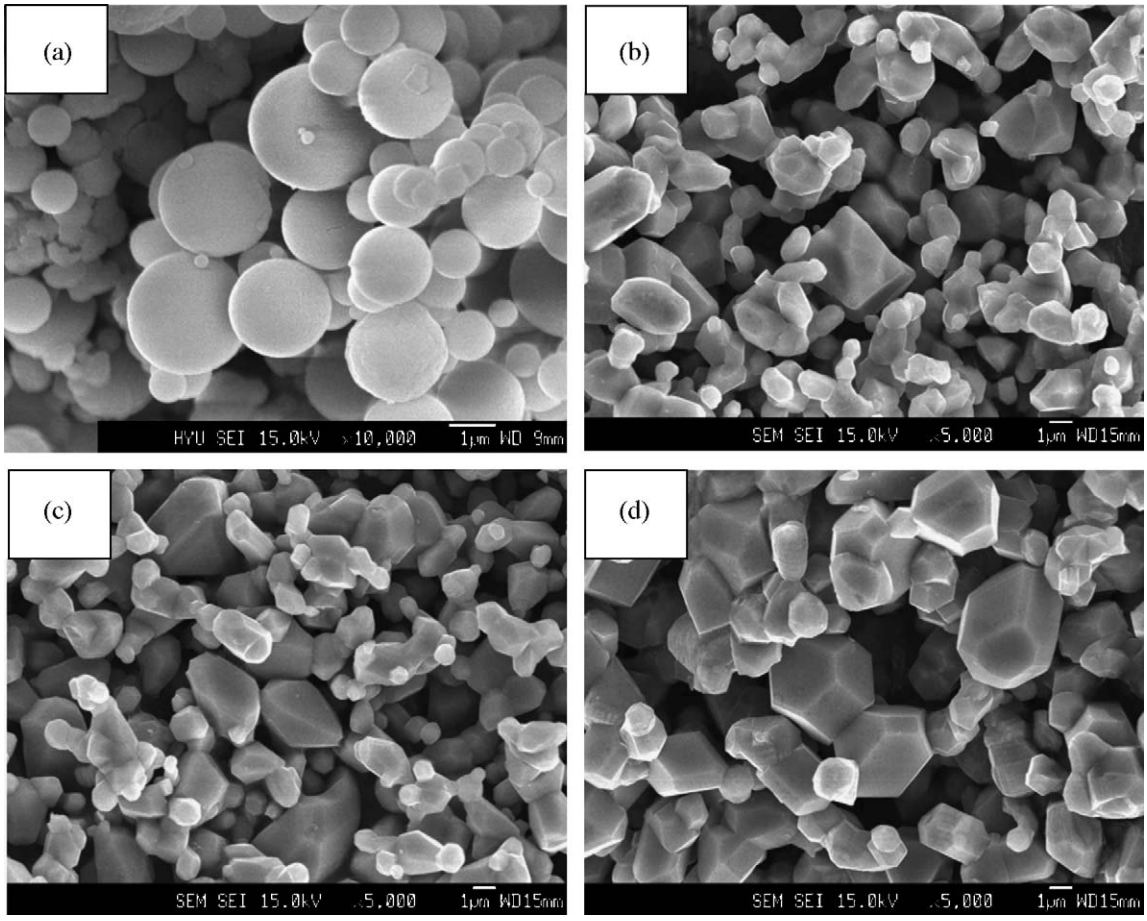

Fig. 1. Scanning election micrographs of $LiNi_{0.5}Mn_{1.5}O_{4-x}F_x$ powders: (a) $Ni_{0.5}Mn_{1.5}O_y$, (b) $LiNi_{0.5}Mn_{1.5}O_4$, (c) $Li[Ni_{0.5}Mn_{1.5}]O_{3.95}F_{0.05}$, (d) $Li[Ni_{0.5}Mn_{1.5}]O_{3.9}F_{0.1}$.

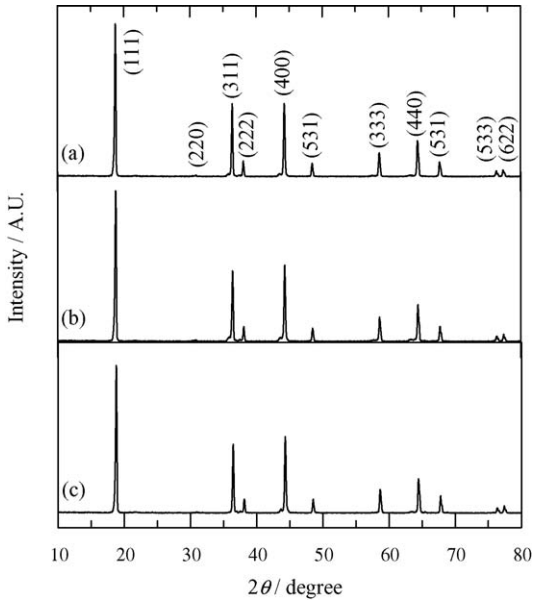

Fig. 2. X-ray diffraction patterns of $LiNi_{0.5}Mn_{1.5}O_{4-x}F_x$: (a) $x=0$, (b) $x=0.05$, (c) $x=0.1$.

ing the refinement. The Rietveld refinement results are shown in Table 1. The fluorine-free $LiNi_{0.5}Mn_{1.5}O_4$ has a lattice parameter of $a=8.172$ Å, while the fluorine-substituted counterparts have $a=8.169$ Å for $x=0.05$ and $a=8.170$ Å for $x=0.1$. The variation in lattice parameters suggests that fluorine ions are successfully substituted for oxygen sites in $LiNi_{0.5}Mn_{1.5}O_4$. The slight decrease of lattice parameter at $x=0.05$ could be due to the smaller ionic radius of F^- ($r=1.33$ Å) compared with that of O^{2-} ($r=1.40$ Å) [23]. Meanwhile, $LiNi_{0.5}Mn_{1.5}O_{3.9}F_{0.1}$ has a slightly larger lattice parameter than $LiNi_{0.5}Mn_{1.5}O_{3.95}F_{0.05}$; 8.169 Å for $x=0.05$ and 8.170 Å for $x=0.1$. Although the lattice parameters do not differ greatly because of the small amount of fluorine, it can be concluded that the slight increase in lattice parameter is attributed to partial $Mn^{4+/3+}$ reduction. With increasing flu-

Table 1
Refinement results of XRD of $LiNi_{0.5}Mn_{1.5}O_{4-x}F_x$ ($x=0$–0.1) based on space groups of $Fd\bar{3}m$

Powder	a (Å)	Vol. (Å^3)	R_{wp} (%)	R_{Bragg} (%)
$LiNi_{0.5}Mn_{1.5}O_4$	8.172	545.803	18.5	3.88
$LiNi_{0.5}Mn_{1.5}O_{3.95}F_{0.05}$	8.169	545.216	18.3	3.96
$LiNi_{0.5}Mn_{1.5}O_{3.9}F_{0.1}$	8.170	545.347	19.0	3.49

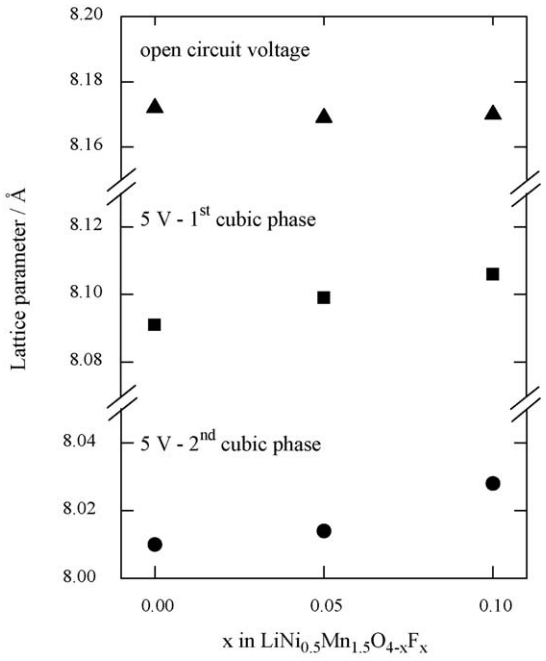

Fig. 3. Variation of lattice parameter, a, from open-circuit voltage to 5 V state in $Li_{\delta}Ni_{0.5}Mn_{1.5}O_{4-x}F_x$; $\delta = 0.05$ for $x = 0$, $\delta = 0.07$ for $x = 0.05$, $\delta = 0.08$ for $x = 0.1$, respectively.

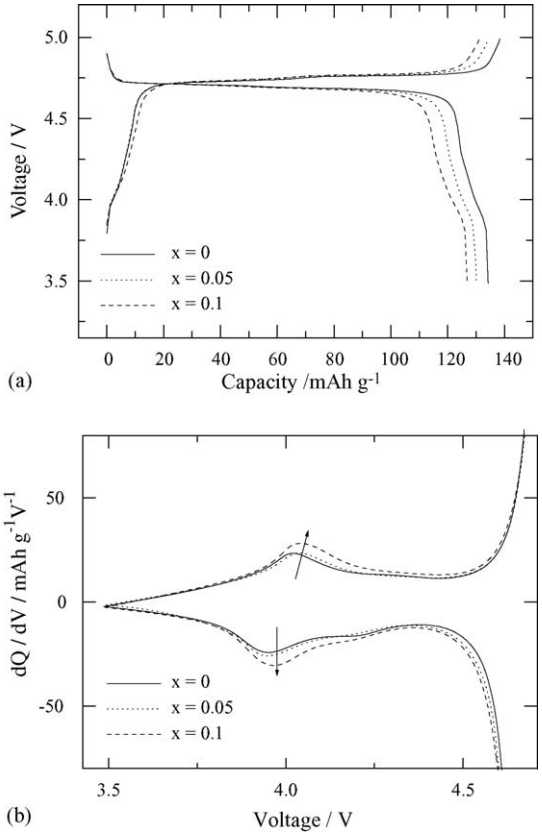

Fig. 4. (a) Voltage profiles and (b) expanded dQ/dV curves of $Li/LiNi_{0.5}Mn_{1.5}O_{4-x}F_x$ cells.

orine content, x, Mn^{4+} ($r = 0.53$ Å) could be reduced to Mn^{3+} ($r = 0.645$ Å) for a stoichiometry of compound. The small ionic radius of F^- would be offset by the large Mn^{3+} ions, which in turn results in the increase in lattice parameter. The electrochemical data support the our assumption in Fig. 4(b) that is discussed later. Xiaomei et al. [24] and Amatucci et al. [19] also reported an increase in the lattice parameter, a, with increasing fluorine content in $LiAl_{1/12}Mn_{23/12}O_{4-z}F_z$ and $LiAl_{0.2}Mn_{1.8}O_{4-z}F_z$.

On charging, the structure of the $Li_{\delta}[Ni_{0.5}Mn_{1.5}]O_{4-x}F_x$ spices is observed from the open-circuit voltage (OCV) valves to 5 V. With Li^+ extraction from the host structures, the XRD patterns with pure-cubic phase shift to higher degrees (2θ), which indicates a decrease in lattice parameter, a. As Li^+ extraction proceeds to more than 80%, another cubic phase appears at higher degrees than the pristine cubic phase. This result is consistent with previous reports that $LiNi_{0.5}Mn_{1.5}O_4$ with a space group of $Fd\bar{3}m$ undergoes a topotactic two-phase transition during Li^+ insertion/extraction [25–27]. The pristine and the newly formed cubic phases are defined here as the first and second cubic phase, respectively. As the two cubic phases coexist at the 5 V charged state, their individual lattice parameters can be calculated by the least-squares method. The individual lattice parameters at 5 V are compared with the values at open-circuit-voltage (OCV) in Fig. 3. The fluorine-free sample shows the largest variation in lattice parameter between OCV and 5 V, i.e., a decrease from 8.172 to 8.091 Å for the first cubic phase, and to 8.01 Å for the second one. With increasing fluorine content, however, the variations in lattice variation is smaller For $Li_{0.08}[Ni_{0.5}Mn_{1.5}]O_{3.9}F_{0.1}$, the lattice parameter decreases from 8.170 to 8.106 Å for the first cubic phase and to 8.028 Å for the second one. These results indicate that a small amount of fluorine substitution effectively reduces the lattice variation in the host structure. Although more experimental evidence is required to reveal an exact mechanism of fluorine effect, it can be speculated that the stronger Li–F bond (577 kJ mol^{-1}) compared with Li–O (341 kJ mol^{-1}) could hinder the extraction of Li^+ ions from the host structure, which in a turn results in the decrease in lattice variation at 5 V [28].

The electrochemical properties of $Li/LiNi_{0.5}Mn_{1.5}O_{4-x}F_x$ cells were studied. The charge and discharge curves of $Li/LiNi_{0.5}Mn_{1.5}O_{4-x}F_x$ cells ($x = 0$–0.1) on the fifth cycle are given in Fig. 4(a). Though fluorine-free $Li/LiNi_{0.5}Mn_{1.5}O_4$ has a discharge capacity of 134 mAh g^{-1}, fluorine-substituted samples show 130 mAh g^{-1} for $x = 0.05$ and 127 mAh g^{-1} for $x = 0.1$. It is notable that $Li/LiNi_{0.5}Mn_{1.5}O_{4-x}F_x$ cells have smaller discharge capacities than that of the fluorine-free one. This again confirms the suggestion that strong Li–F bonding can hinder Li^+ extraction from the host structure. An expanded view of the dQ/dV curves of $Li/LiNi_{0.5}Mn_{1.5}O_{4-x}F_x$ cells is presented in Fig. 4(b). All samples exhibit 4-V capacities that grow with increasing fluorine content. The 4-V capacities are due to the $Mn^{3+/4+}$ redox [19], and therefore an increase in 4-V

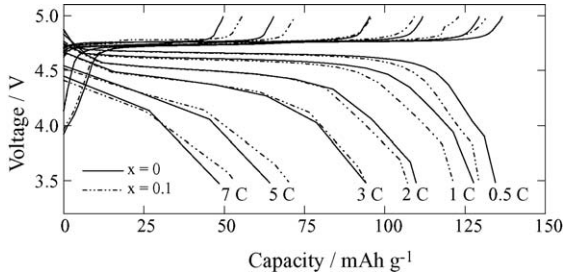

Fig. 5. Normalized discharge capacities vs. number of cycles at different current densities between 3.5 and 5.0 V. Cells charged using constant current density of 27 mA g^{-1} (0.2 C-rate).

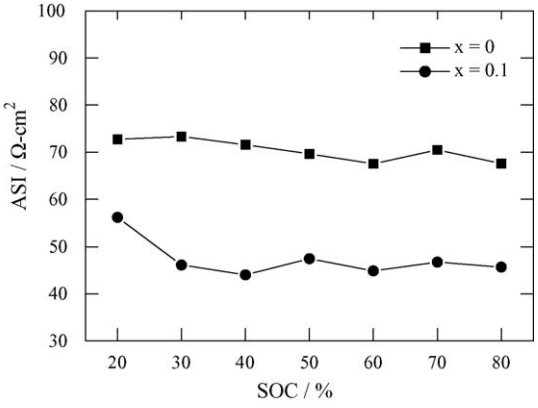

Fig. 6. Area-specific impedance (ASI) vs. state-of-discharge (SoD) of Li/$LiNi_{0.5}Mn_{1.5}O_{4-x}F_x$ cells: (a) $x = 0$, (b) $x = 0.05$, (c) $x = 0.1$.

capacity means an increasing amount of Mn^{3+} ions in the fluorine-substituted samples. This result supports the previous assumption that $Mn^{4+/3+}$ reduction is due to fluorine substitution in $LiNi_{0.5}Mn_{1.5}O_{4-x}F_x$.

The effect of F substitution on the 0.5–7 C-rate capability between 3.5 and 5.0 V is demonstrated in Fig. 5. The Li/$LiNi_{0.5}Mn_{1.5}O_{4-x}F_x$ ($x = 0$ and 0.1) cells were charged with a constant current density of 27 mA g^{-1} (0.2 C-rate) before each discharge test. Bare $LiNi_{0.5}Mn_{1.5}O_4$ exhibits higher discharge capacities than $LiNi_{0.5}Mn_{1.5}O_{3.9}F_{0.1}$ at low C-rates. Above a rate of more than 3 C, however, $LiNi_{0.5}Mn_{1.5}O_{3.9}F_{0.1}$ displays better capacity retention than an unsubstituted sample. The small variation in lattice parameters is beneficial for rate capability because of the small structural strain during repetitive Li^+ insertion/extraction. From this point of view, it is considered that Li/$LiNi_{0.5}Mn_{1.5}O_{3.9}F_{0.1}$ is advantageous for high-rate cycling.

To understand the superior rate capability of fluorine-substituted samples, the area-specific impedance (ASI) was measured as a function of the state-of-discharge (SOD) at 30 °C. During lithium insertion/extraction, a combination of electrode kinetics, ohmic drop and Li^+ ion diffusion through the electrolyte and within electrode cause a change in the overall cell voltage [29]. The area-specific impedance (ASI) was determined by $(A \cdot \Delta V)/I$, where A is the cross-sectional area of the electrode (2 cm^2), ΔV is the voltage variation during current interruption for 60 s at each SOD, and I is a constant current density of 0.2 mA cm^{-2} that is applied during galvanostatic cycling. The $LiNi_{0.5}Mn_{1.5}O_{3.9}F_{0.1}$ electrodes exhibit lower ASI values than the $LiNi_{0.5}$ $Mn_{1.5}O_4$ electrode, as shown in Fig. 6, the ASI values are the 76 and 53 Ω cm^2 for $x = 0$ and 0.1, respectively. This finding suggests that fluorine substitution in $LiNi_{0.5}$ $Mn_{1.5}O_4$ can enhance Li^+ ion diffusion. In the charge–discharge process, Li^+ ions transfer between a cathode material (solid phase) and an electrolyte solution (liquid phase). The solvation/desolvation of Li^+ ions occurs at the surface of the active material because Li^+ ions are in a solvated state in an electrolyte solution. Since the metal–fluoride (M–F) bond is more polarized than the metal–oxygen (M–O) bond, the affinity for a polar electrolyte solution may be improved at the fluorinated surface of the active material [30]. Therefore, the transfer of Li^+ ions between the solid and the liquid phase may easily proceed.

The effect of fluorine substitution on the stability of cathode material against HF attack has been investigated. The HF is produced by hydrolysis of the supporting salts such as $LiPF_6$ with a small amount of residual water contained in the electrolyte solution. The HF attacks the M–O bond and water is reproduced, so that the reaction is self-sustaining. A constant amount of $LiNi_{0.5}Mn_{1.5}O_{4-x}F_x$ ($x = 0$–0.1) powders was stored in dilute HF solution at 60 °C for 1 week after which the concentrations of Ni and Mn ions were measured by AAS and are listed in Table 2. Fluorine-substituted samples display better resistance against HF attack in that they show lower concentrations of Ni and Mn in the electrolyte than those for the fluorine-free sample. Although the exact mechanism has yet to be understood, it is proposed that a fluorine coating effectively reduces dissolution of particles into the electrolyte [31,32]. In addition, a decrease in the contact area between the fluorine-substituted particles and the HF solution could partly contribute to the suppression of metal dissolution.

The thermal stability of positive materials, especially in a delithiated state, is an important factor in assessing their suitability for practical application in lithium secondary batteries. The DSC profiles of $Li_\delta Ni_{0.5}Mn_{1.5}O_{4-x}F_x$ ($x = 0$–0.1) electrodes charged to 5.0 V, are given in Fig. 7. The $Li_{0.05}Ni_{0.5}Mn_{1.5}O_4$ electrode has an abrupt exothermic peak at around 238.3 °C (1958 J g^{-1}). Meanwhile, as the

Table 2
Dissolved Ni and Mn concentration in diluted HF solution at 60 °C for 1 week

Powder	Ni dissolution (ppm)	Mn dissolution (ppm)
$LiNi_{0.5}Mn_{1.5}O_4$	65.3	71.5
$LiNi_{0.5}Mn_{1.5}O_{3.95}F_{0.05}$	48.5	47.2
$LiNi_{0.5}Mn_{1.5}O_{3.9}F_{0.1}$	44.0	44.2

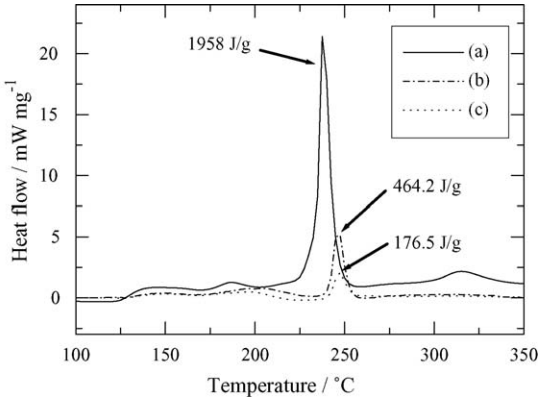

Fig. 7. Differential scanning calorimetry (DSC) profiles of $LiNi_{0.5}Mn_{1.5}O_{4-x}F_x$ electrodes at 5.0 V: (a) $x=0$, (b) $x=0.05$, (c) $x=0.1$.

Table 3
Surface area (calculated using BET isotherm) of $LiNi_{0.5}Mn_{1.5}O_{4-x}F_x$ ($x=0$–0.1) powders

Powder	Surface area ($m^2\ g^{-1}$)
$LiNi_{0.5}Mn_{1.5}O_4$	3.79
$LiNi_{0.5}Mn_{1.5}O_{3.95}F_{0.05}$	1.21
$LiNi_{0.5}Mn_{1.5}O_{3.9}F_{0.1}$	0.98

fluorine content increases, $Li_\delta Ni_{0.5}Mn_{1.5}O_{4-x}F_x$ electrodes exhibits smaller exothermic peaks at higher onset temperatures than fluorine-free electrode, i.e., 246.3 °C (464.2 J g^{-1}) for $x=0.05$ and 246.7 °C (176.5 J g^{-1}) for $x=0.1$. The decrease in exothermic heat amount with increasing fluorine content can be attributed to a decrease of the contact area between the particles and the electrolyte. As the surface area of the powders is decreased by fluorine substitution (Table 3), the contact area also decreases. Similar studies [31,33] have shown that fluorine substitution for oxygen significantly improves the thermal stability of $Li[Ni_{1/3}Co_{1/3}Mn_{1/3}]O_{2-z}F_z$ with an increase in particle size. In summary, it is concluded that fluorine substitution is advantageous for the thermal stability of $Li_\delta Ni_{0.5}Mn_{1.5}O_{4-x}F_x$ spinel.

4. Conclusion

$LiNi_{0.5}Mn_{1.5}O_{4-x}F_x$ ($0 \le x \le 0.1$) spinel powders have been prepared via an ultrasonic spray pyrolysis method. An investigation has been made of the effect of fluorine on the structure, morphology, thermal stability and electrochemical properties of $LiNi_{0.5}Mn_{1.5}O_{4-x}F_x$. All $LiNi_{0.5}Mn_{1.5}O_{4-x}F_x$ ($0 \le x \le 0.1$) materials have a phase-pure spinel structure with a space group of $Fd\bar{3}m$. During Li^+ extraction, $LiNi_{0.5}Mn_{1.5}O_{4-x}F_x$ experiences a smaller lattice variation than bare $LiNi_{0.5}Mn_{1.5}O_4$ and this enhances the rate capability at high C-rates. In addition, $LiNi_{0.5}Mn_{1.5}O_{3.9}F_{0.1}$ exhibits a lower area specific in pedance that than of $LiNi_{0.5}Mn_{1.5}O_4$. A small amount of fluorine substitution for oxygen give rise to a small variation in lattice parameter, as well as reduced Ni and Mn dissolution from HF attack which, in turn, enhances the electrochemical properties and thermal stability. This is partly due to a decrease in the surface area of the powders by fluorine substitution.

Acknowledgement

This research was supported by the Hanyang University IT Research Center Project.

References

[1] T. Ohzuku, M. Kitagawa, T. Hirai, J. Electrochem. Soc. 137 (1990) 769.
[2] J.M. Tarascon, E. Wang, F.K. Shokooki, W.R. Mckinnon, S. Colson, J. Electrochem. Soc. 138 (1990) 2858.
[3] R.J. Gummow, A. de Kock, M.M. Thackeray, Solid State Ionics 69 (1994) 59.
[4] K. Amine, H. Tukamoto, H. Yasuda, Y.A. Fujita, J. Electrochem. Soc. 143 (1996) 1607.
[5] M.M. Thackeray, Y. Shao-Horn, A.J. Kahaian, Electrochem. Solid-State Lett. 1 (1998) 7.
[6] Y. Xia, Y. Zhou, M. Yoshio, J. Electrochem. Soc. 144 (1997) 2593.
[7] P. Arora, B.N. Popov, R.E. White, J. Electrochem. Soc. 145 (1998) 807.
[8] R.J. Gummow, A. de Kock, M.M. Thackeray, Solid State Ionics 69 (1994) 59.
[9] L. Gouhua, H. Ikuta, T. Uchida, M. Wakihara, J. Electrochem. Soc. 143 (1996) 178.
[10] H. Kawai, M. Nagata, H. Tukamoto, A.R. West, J. Power Sources 81–82 (1999) 67.
[11] Y. Ein-Eli, W.F. Howard Jr., S.H. Lu, S. Mukerjee, J. McBreen, J.T. Vaughey, M.M. Thackeray, J. Electrochem. Soc. 145 (1998) 1238.
[12] C. Sigala, D. Guyomard, A. Verbaere, Y. Piffard, M. Tournorx, Solid State Ionics 81 (1995) 167.
[13] K. Amine, H. Tukamoto, H. Yasuda, Y. Fujita, J. Electrochem. Soc. 143 (1996) 1607.
[14] Q. Zhong, A. Bonakdarpour, M. Zhang, Y. Gao, J.R. Dahn, J. Electrochem. Soc. 144 (1997) 205.
[15] K. Kanamura, W. Hoshikawa, T. Umegaki, J. Electrochem. Soc. 149 (2002) A339.
[16] Y.-K. Sun, Y.-S. Jeon, H.-J. Lee, Electrochem. Solid-State Lett. 3 (2000) 7.
[17] S.-H. Park, K.-S. Park, Y.-K. Sun, K.-S. Nahm, J. Electrochem. Soc. 147 (2000) 2116.
[18] Y.-S. Lee, M. Yoshio, Electrochem. Solid-State Lett. 4 (2001) A85.
[19] G.G. Amatucci, N. Pereira, T. Zheng, J.-M. Tarascon, J. Electrochem. Soc. 148 (2001) A171.
[20] T. Roisnel, J. Rodriguez-Carjaval, Fullprof Manual, Institute Laue-Langevin, Grenoble, 2000, p. 13.
[21] S.-H. Park, S.-W. Oh, S.-T. Myung, Y.C. Kang, Y.-K. Sun, Solid State Ionics 176 (2005) 481.
[22] G.-H. Kim, S.-T. Myung, H.J. Bang, J. Prakash, Y.-K. Sun, Electrochem. Solid-State Lett. 7 (2004) A477.
[23] J.A. Dean, Langes's Handbook of Chemistry, vol. 4.5.1–4.5.3, 15th ed., McGraw-Hill Inc., USA, 1999.
[24] W. Xiaomei, Z. Xiangfu, Y. Qinghe, J. Zhongkao, W. Haoqing, J. Fluorine Chem. 107 (2001) 39.
[25] S.-T. Myung, S. Komaba, N. Kumagai, H. Yashiro, H.-T Chung, T.-H. Cho, Electrochim. Acta 47 (2002) 2543.
[26] J.-H. Kim, C.S. Yoon, S.-T. Myung, J. Prakash, Y.-K. Sun, Electrochem. Solid-State Lett. 7 (2004) 216.

[27] J.-H. Kim, S.-T. Myung, C.S. Yoon, S.G. Kang, Y.-K. Sun, Chem. Mater. 16 (2004) 906.
[28] David R. Lide, Editer-in-chief CRC Handbook of Chemistry and Physics, vol. 9-54-55, 77th ed., CRC-Press Inc., 1996.
[29] Q. Wu, W. Lu, J. Prakash, J. Power Sources 88 (1999) 237.
[30] S. Yonezawa, M. Yamasaki, M. Takasima, J. Fluorine Chem. 125 (2004) 1657.
[31] G.-H. Kim, J.-H. Kim, C.S. Yoon, S.-T. Myung, Y.-K. Sun, J. Electrochem. Soc. 152 (2005) 1707.
[32] Yonekawa Fumihiro, Ota Hirokuni, Yamazaki Nobuyuki, Japanese Patent 2003-221235 (2003).
[33] G.-H. Kim, S.-T. Myung, H.J. Bang, J. Prakash, Y.-K. Sun, Electrochem. Solid-State Lett. 7 (2004) A477.